and found that, even in a temperature-controlled chamber, the unit required a ~2 h warmup before it stabilized. Some newer OSA units contain an internal wavelength reference such as an acetylene absorption cell.

Wavelength meters that measure a signal's wavelength relative to a built-in fundamental reference (often a helium-neon laser operating at the 632.991 nm vacuum wavelength) usually don't require frequent calibration. The most convenient way to check a wavelength meter is to measure a laser that has a known wavelength, such as the 1523.488 nm helium-neon laser (~1 part in 10^6 absolute stability) or a laser that is stabilized to a fundamental reference. Alternatively, a tunable laser can be tuned over an absorption line while measuring the wavelength with a wavelength meter; the measured line center can then be compared with the true line center.

In all of these cases, it is important to use the wavelength of light in vacuum, rather than the wavelength in air, when calibrating equipment. The wavelength of light in air can vary substantially due to its dependence on the atmospheric pressure, temperature, and humidity.

5. Conclusions

There are a variety of convenient wavelength calibration standards in the 1500 nm region, and other standards are under development for the WDM L-band. Fundamental references based on atomic and molecular absorption or emission lines provide the highest accuracy, but they are not available in all wavelength regions. Wavelength division multiplexing will likely expand into the 1300 and 1400 nm regions, and it will be very difficult to find absolute references for this wide wavelength range. Artifacts such as etalons or fiber Bragg gratings can provide references at arbitrary wavelengths, but they can suffer from large sensitivity to temperature, strain, and pressure. Passive or active thermal stabilization can substantially reduce this variability, but the artifact references need to be checked periodically against a fundamental reference. Further in the future, stabilized frequency combs may become commercially available to provide frequency (wavelength) markers throughout the WDM regions.

References

1. S.L. Gilbert, "Frequency Stabilization of a Fiber Laser to Rubidium: a high accuracy 1.53 μm wavelength standard," in *Frequency Stabilized Lasers and Their Applications*, Proc. SPIE 1837, 146–153 (1993).
2. Y.C. Chung, "Frequency-Locked 1.3- and 1.5-μm Semiconductor Lasers for Lightwave Systems Applications," J. Lightwave Technol. 8, 869–876 (1990).
3. U. Fischer and C. von Helmolt, "Absorption Spectra of Excited Kr 84 States between 1.5 and 1.58 μm and Their Use for Absolute Frequency Locking," J. Lightwave Technol. 14, 139–143 (1996).
4. A. Bruner et al., "Frequency stability at the kilohertz level of a rubidium-locked diode laser at 192.114 THz," Appl. Opt. 37, 6410–14 (1998).
5. D.A. Humphreys, "Accurate wavelength calibration for optical spectrum analyzers," in *Technical Digest—Symposium on Optical Fiber Measurements*, Natl. Inst. Stnd. Technol. Spec. Publ. 905, pp. 97–100 (1996).
6. W.C. Swann and S.L. Gilbert, "Pressure-induced shift and broadening of 1510–1540-nm acetylene wavelength calibration lines," J. Opt. Soc. Am. B 17, 1263–1270 (2000); S.L. Gilbert and W.C. Swann, "Acetylene $^{12}C_2H_2$ Absorption Reference for 1510 nm to 1540 nm Wavelength Calibration—SRM 2517a," Natl. Inst. Stnd. Technol. Spec. Publ. 260–133 (2001 Edition).
7. S.L. Gilbert, W.C. Swann, and C.M. Wang, "Hydrogen Cyanide $H^{13}C^{14}N$ Absorption Reference for 1530–1560 nm Wavelength Calibration-SRM 2519," Natl. Inst. Stnd. Technol. Spec. Publ. 260–137 (1998).
8. Y. Kokubun et al., "Athermal Waveguides for Temperature-Independent Lightwave Devices," Photon. Technol. Lett. 5, 1297–1300 (1993).
9. T. Iwashima et al., "Temperature compensation technique for fibre Bragg gratings using liquid crystalline polymer tubes," Electron. Lett. 33, 417–419 (1997).
10. W.C. Swann et al., "Hybrid multiple wavelength reference using fiber gratings and molecular absorption," in *Proc., Bragg Gratings, Photosensitivity, and Poling in Glass Waveguides*, OSA Technical Digest (Optical Society of America, Washington DC, 1999), pp. 63–65.
11. V. Bertogalli et al., "Testing passive DWDM components: uncertainties in swept-wavelength measurement systems," in *Proc., 2001 Optical Fiber Communication Conference* (Optical Society of America, Washington DC, 2001), paper THB6.
12. M. Maleki and J.C. Petersen, "Wavelength calibration of a fiber-optical spectrum analyzer: temperature dependence," Appl. Opt. 36, 4451–4455 (1997).

ThC2 **9:00 am**

Wavelength monitoring of tunable DWDM sources using a FP etalon and a FP laser diode

Chun-Liang Yang and San-Liang Lee, *Dept. of Electronic Engineering, National Taiwan University of Science and Technology, 43, Keelung Rd,. Sec. 4, Taipei, Taiwan 106, R.O.C., Email: Sanlee@et.ntust.edu.tw*

1. Introduction

Tunable laser sources are critical components for DWDM networks as spare sources or fast wavelength-switching devices. The wavelength monitor for controlling a tunable laser diode must cope with multiple output wavelengths and the required tuning speed. Fabry-Perot (FP) etalons have been commercially used for wavelength control of DWDM lasers. However, a FP etalon cannot distinguish among different channels since it has periodic wavelength characteristic. This makes it difficult to monitor the mode-hopping problem that might happen in tuning a tunable laser.[1] Etalons with special tuning mechanism or array waveguide gratings were also proposed to monitor tunable lasers,[2,3] but they may have limited response speed or require expensive components. On the other hand, wavelength monitoring by detecting the transparent current or the induced junction voltage across a FP laser diode (FPLD) was demonstrated to provide 0.01-nm wavelength resolution.[4] This approach is very attractive since the wavelength sensor can be monolithically integrated with the tunable laser. Moreover, a FPLD can easily be tuned to monitor multiple channels by adjusting its bias current. However, to achieve 0.01-nm resolution with this approach requires tough stability on temperature control.

We propose here a high-resolution tunable wavelength monitoring technique that combines the advantages of stable temperature properties of a FP etalon filter as well as fast tunability of the transparent properties of a FPLD. Significant relief to the required temperature stability, about ±0.2°C, is achieved, so wavelength resolution of 0.01 nm can easily be obtained for many channels. The ambiguity among different channels for the etalon can be resolved from the induced voltage across the LD. This technique can also be applied in optical networking units to monitor the wavelength paths in a scanning mode.

2. Operation principles

Fig. 1 shows the schematic of the proposed wavelength monitoring technique for tunable laser module. The laser output is first collimated and dithered at a specific frequency with an optical modulator. Then, the signal is divided into two paths, one to an FP etalon, and the other to a FPLD. Both the transmitted and reflected signals of the etalon are measured and the resultant differential voltage or voltage ratio for these two signals are used for detecting the wavelength drift from the wavelength grid. The FPLD can resolve the wavelength channel from either the corresponding transparent current or the junction voltage.

The tunable laser light is dithered in order to improve the detected signal quality for both monitoring paths. For easy packaging with the tunable laser in a compact module, a surface-normal type of modulator is favored to simplify light coupling. Since the required dithering frequency is between kHz and MHz, modulators made of liquid crystal or micromechanical silicon modulator[5] are among the good choices for such applications.

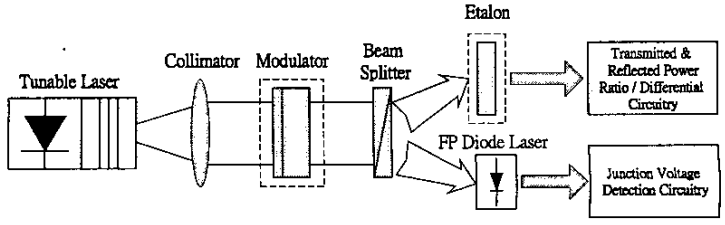

ThC2 Fig. 1. Schematic of wavelength monitoring for a tunable laser.

3. Experimental demonstration

The proposed method exploits the FP etalon as both a wavelength locker and a stable wavelength reference because of its stable response to ambient temperature variation. Fig. 2(a) depicts the reflected and transmitted characteristics of an etalon of which the cavity length is specially designed to give rise to a free-spectral range (FSR) of 50 GHz. The intersection point of the transmitted and reflected curves is frequency used as the monitoring point. Fig. 2 shows that the point varies at a rate of 0.011 nm/°C as the temeprature changes. If the tolerance on wavelength deviation is 0.01 nm, this etalon can tolerate up to 0.9°C of temperature change. The etalon was temperature-controlled to align one of the ITU wavelengths to a specific crossing point of the two curves. Fig. 2 shows the response for the etalon to eight wavelengths of 100-GHz channel spacing at the same temperature, 26°C. Since the chanel spacing matches twice the FSR, the responses to wavelength drift are almost identical among the channels. Therefore, the monitoring circuit needs to memorize only one of these curves. The maximal deviation among the curves results in 0.005 nm of wavelength deviation, which is much smaller than the channel spacing.

As the tunable laser is tuned to output a given DWDM wavelength, the etalon must monitor the wavelength deviation from the wavelength grid and feedback the deviation to the laser control unit to adjust the wavelength to the closest wavelength grid. Then, the FPLD will recognize the channel and detect if mode hopping occurs. Two modes of opertion for the FPLD can be performed for channel recognition. One is to sweep the bias current and locate the transparent current (I_{tr}) for the incident wavelength (λ), and the other is to detecte the induced junction voltage across the diode for a fixed bias current. Fig. 3 shows the wavelength-dependent characteristics

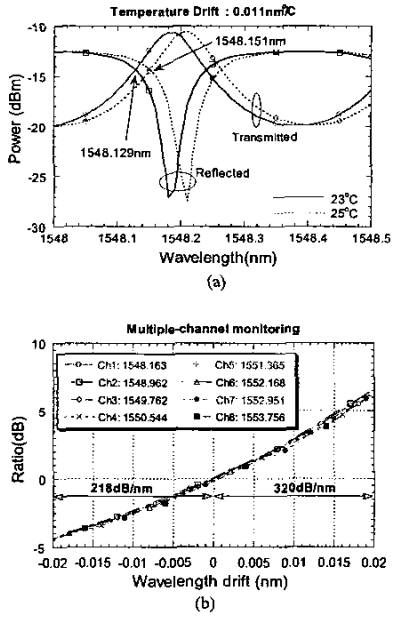

ThC2 Fig. 2. Characteristics of the FP etalon: (a) at different temperature and (b) around eight ITU wavelengths.

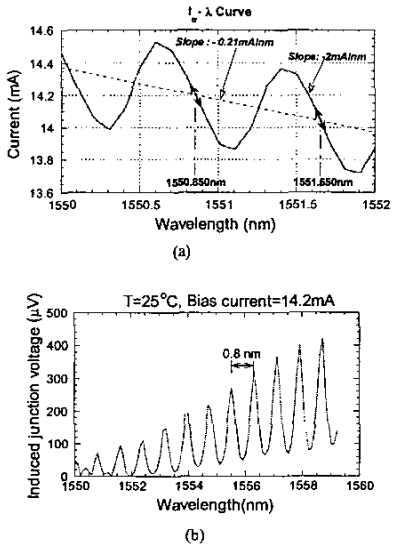

ThC2 Fig. 3. Wavelength variation of transparent current (a) and junction voltage (b) for a FPLD.

for a 1.55-μm FPLD. For a SOA, the transparent current decreases as the wavelength moves to the long-wavelength side. On the other hand, due to the facet reflection, resonant effects appear in the wavelength variation of transparent current and induced voltage. The wavelength spacing between the resonant peaks is equal to the cavity mode spacing of the LD. Here, we chose a FPLD of which the cavity mode spacing is very close to 100 GHz (0.8 nm).

Although it is desired to have a montonic I_{tr}-vs-λ curve, which can be obtained from a SOA, the resonant effects can enhance the wavelength resolution. It was also found in the experiments that the induced junction voltage across a FPLD is larger than that across a SOA. For monitoring a DWDM tunable laser, the resonant characteristics can be used if the cavity mode spacing is identical to the channel spacing. After the wavelenth is aligned to the wavelength grid, only the discrete points spaced by the channel spacing will be used for channel recognition. The curve can easily be adjusted by changing the diode temperature to align the wavelength grid to the middle of the slope, as indicated in Fig. 3. The transparent current differs by 0.16 mA between the adjacent channels. The tolerance on temperature control of the FPLD is relaxed to ±0.2°C because the transparent current varies by 0.385 mA/°C with the temperature. This benefits again from the use of the FP etalon as a wavelength reference. Moreover, the deviation of the transparent current from the value for a wavelength grid can indicate the temperature shift and serve as the control signal for stabilizing the temperature.

Detecting the junction voltage may be favored for monitoring fast tunable lasers since it has a faster response than locating the transparent current. Fig. 4 demonstrates a tunable wavelength monitoring with a combination of a FP etalon and a FPLD. A commercial tunable laser was tuned to eight DWDM channels in a step of 0.8 nm. The junction voltage of the FPLD changes in a stair way in response to the wavelength tuning.

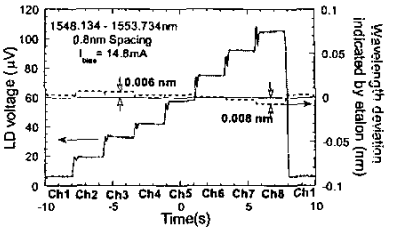

ThC2 Fig. 4. Tunable monitoring of eight 100-GHz channel The monitored light is modulated at 1 kHz.

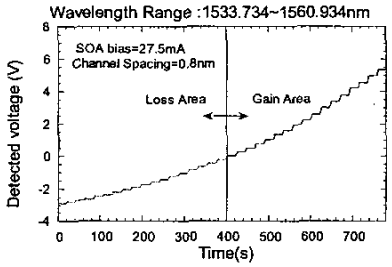

ThC2 Fig. 5. Output voltage of SOA for 35 channels. The induced voltage was amplified by 2 × 10^5.

Tiny signal appears at the output of the etalon circuit since the wavelengths are allocated at the wavelength grid. The etalon signal indicates a maximal wavelength deviation of 0.008 nm, which is acceptable for DWDM channels of 100-GHz spacing.

4. Discussion

For monitoring a widely tunable laser that can output more than 30 channels, a FPLD might suffer from the resonant characteristics if the cavity mode spacing is not exactly equal to the channel spacing. In such cases, a SOA with monotonic wavelength variation of transparent current and junction voltage is needed. Fig. 5 shows the output signal as the tunable laser is tuned over 35 channels. The channel wavelengths can be clearly resolved from the junction voltage. In the experiments, the SOA is biased at the transparent current for the 1548.134-nm channel. Phase-sensitive detection is employed to obtain the voltage such that the channels reside in the gain region of the SOA can be distinguished from those in loss region. A SOA for this application can be low-cost since it does not require tough anti-reflection coating as required for conventional applications. Noting that, as a SOA is used, the mode hopping or wavelength channels can be determined from the junction voltage without waiting for the etalon to bring the wavelength to the closest wavelength grid.

References

1. D.A. Ackerman, et. al., "Wavelength, modal, and power stabilization of tunable electroabsorption modulated distributed Bragg reflector lasers," in *Int. Semiconductor Laser Conf.*, pp. 49–50, Monterey, CA, 2000.
2. K. Tatsuno et al., "50 GHz spacing, multiwavelength tunable locker integrated in a

transmitter module with a monolithic-modulator and a DFB laser," *OFC 2001,* Anaheim, USA, paper TuB5, 2001.
3. K.R. Tamura et al., "32 wavelength tunable mode-locked laser with 100 GHz channel spacing using an arrayed waveguide grating," *OFC 2001,* Anaheim, USA, paper TuJ5, 2001.
4. S.-L. Lee, et al., "High-resolution wavelength monitoring using differential/ratio detection of junction voltage across a diode laser," *IEEE Photon. Technol. Lett.,* vol. 13, pp. 872–874, 2001.
5. K.W. Goosen, et al., "Silicon modulator based on mechanically-active anti-reflection layer with 1 Mbit/sec capability for fiber-in-the-loop applications," *IEEE Photon. Technol. Lett.,* vol.6, pp. 1119–1121, 1994.

ThC3 **9:15 am**

Birefringent Gires-Tournois Interferometer (BGTI) for DWDM Interleaving

S. Cao, C. Lin, C. Yang, E. Ning, J. Zhao and G. Barbarossa, *Avanex Corporation, 40919 Encyclopedia Circle, Fremont, CA 94538, Email: christopher_lin@avanex.com*

1. Introduction

Interleavers enable the practical implementation of dense wavelength division multiplexing (DWDM) systems by transforming the task of separating or combining a single set of very closely spaced channels into separating or combining multiple sets of widely spaced channels. Regardless of the approach, be it thin-film filter, fiber-Bragg grating, arrayed waveguide grating, Echelle grating, or bulk diffraction grating, mux/demux modules can be less expensive and easier to make if the channel spacing is wide relative to the required passband width. Interleavers allow the application of these wide channel spacing solutions to the harder problem of more closely spaced channels. Most interleaver designs are based on cascaded Mach-Zehnder (M-Z) interferometers. Researchers have constructed these cascaded M-Z interleavers out of fused fibers and planar lightwave circuits for example.[1-2] Other, non-M-Z and hybrid-M-Z approaches exist as well.[3]

We propose a Birefringent Gires-Tournois Interferometer (BGTI) that combines the benefits of the nonlinear phase response of Gires-Tournois (G-T) cavities, free space propagation, and low sensitivity to physical layout. This new structure is assembled in a Michelson configuration except that the beam splitter is replaced by a polarization beam splitter (PBS) and the mirrors are replaced by Gires-Tournois (G-T) cavities. Furthermore, 1/8 waveplates are placed between the polarization beam splitter and the G-T cavities in each arm of the interferometer and 1/4 waveplates are placed within the G-T cavities (see figure 1).

The BGTI interleaver possesses four desirable features: low stage count, temperature insensitivity, frequency based periodicity, and fabrication simplicity. The highly nonlinear phase response of G-T cavities enables the BGTI interleaver to accomplish with a single stage what other M-Z designs require two or even three stages to achieve.[1-2] The temperature stability and frequency, as opposed to wavelength, periodicity are derived from the predominantly free-space design. Most of the propagation through the interleaver is through air whose index of refraction dependence on temperature and wavelength is weak. Designs dependent on wavelength periodicity suffer from channel center walk-off at the extreme channels in a DWDM system since the channel grid is defined by frequency. The fabrication simplicity stems from the use of thin, birefringent plates to create the path length differential between the two beams that interfere to produce the interleaver response.

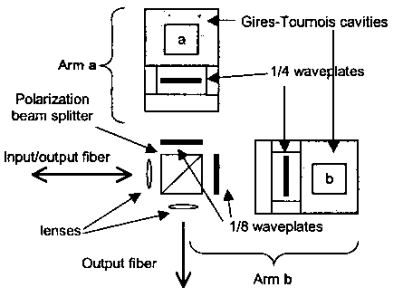

ThC3 Fig. 1. Birefringent Gires-Tournois Interferometer (BGTI) interleaver.

2. Operation of device

Fundamentally, the two outputs of the BGTI interleaver are the sum and difference of the equally weighted outputs of two otherwise identical all-pass filters whose frequency responses are shifted by 1/2 period. A phase delay is added in one arm to provide phase offset adjustment (see figure 2). Madsen provides a description of arbitrary filters based on this type of basic building block.[4]

In the BGTI, the *s* and *p* polarizations defined by the PBS are rotated 45° with respect to the ordinary (*o*) and extraordinary (*e*) axes of the waveplates. The function of the PBS is two-fold. The PBS segregates the incoming *s* and *p* polarizations for separate treatment in the two arms of the BGTI. In conjunction with the waveplates, it also functions as a 50/50 splitter.

Considering only the *p* polarized light, half the power travels along the *e* axes of the two waveplates and the other half travels along the *o* axes due to the 45° rotation of the *p* light with respect to those axes. Upon return to the PBS, the *e* and *o* beams from the waveplates are combined as sum and difference beams and are output in either the *s* or *p* plane defined by the PBS. The operation is similar for the *s* polarized light traveling through the other arm.

The two arms of the interferometer operate independently so that there is no interference between light of the same wavelength from the two arms. The light of a given wavelength traveling back to the PBS from arm **a** is always orthogonal in polarization to the light of the same wavelength from arm **b** (see figure 1). For this reason, the lengths of arms **a** and **b** are inconsequential to the operation of the device and therefore temperature or vibration induced deviation is harmless. In fact, the only reason two arms are included is to accommodate arbitrary input polarization. This does mean that inequality between the lengths of the two arms will produce polarization mode dispersion. However, this effect is small and easy to control.

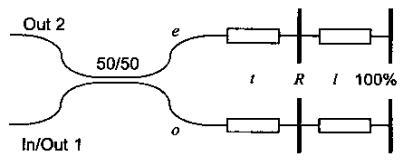

ThC3 Fig. 2. All-pass filter decomposition of a single arm in the BGTI interleaver.

3. Theory

As stated previously, each arm of the BGTI interleaver operates independently of the other and is mathematically identical to the filter shown in figure 2. The phase response of each arm in the filter shown in figure 2 is:

$$\varphi_i = 2k_i t + 2\tan^{-1}\left[\frac{1+\sqrt{R}}{1-\sqrt{R}}\tan(k_i l)\right]$$

where the subscript *i* denotes either the extraordinary or ordinary arm of the filter, k_i is the polarization dependent wavevector, *t* is the thickness of the waveplate outside the cavity, *R* is the power reflectivity of the cavity, and *l* is the cavity length including the waveplate inside the cavity.

Within the cavity, the round trip phase difference between the *e* and *o* arms due to the 1/4 waveplate is π. This ensures a symmetric response in the two output ports. The selection of *R* determines the depth of phase modulation. Large *R* will produce rapid change in the phase response causing a sharp transition from the passband to the stopband. Large *R* will also produce ripple in the passband and chromatic dispersion. Outside the cavity, the round trip phase difference between the *e* and *o*ar ms due to the 1/8 waveplate provides a phase difference bias to produce full range in the response of the two arms.

By manipulating the values of *R*, *t*, and *l*, different filtering functions can be achieved. The BGTI is a basic building block that can be used to build general IIR optical filters as described by Madsen.[4] By adding mirrors and waveplates, higher order all-pass filters can be constructed.

4. Results

The two devices discussed in this paper were built out of discrete, micro-optic components. The G-T cavities were air gap cavities constructed with low thermal expansion spacers. The first device uses *R* = 18.5% mirrors. As shown in figure 3, the calculated and measured responses of the two ports match very well over the passband. However, the two outputs have different isolation. The isolation of port 1 is worse than that of port 2. Moreover, the isolation is worse than calculated in both cases. These features are caused by the imperfect and asymmetric segregation of the *s* and *p* polarizations by the PBS cube. Since the extinction ratios of the transmission and reflection operations of the PBS are unequal, different amounts of crosstalk will leak into each port since the path to each port involves different numbers of transmission and reflection interactions with the PBS. Practically, PBS isolation is typically limited to 30 dB at best. Therefore, the isolation floor of the BGTI is similarly restricted. The 1 dB passband of the device shown in figure 3 is 77 GHz and the insertion loss is less than 1 dB.

In order to improve the cross-port isolation, additional BGTI stages can be added. In figure 4, the output spectra of a two stage BGTI interleaver with *R* = 22.0% for all cavities is shown. Since the